Objective-Oriented Power Quality Compensation of Multifunctional Grid-Tied Inverters and Its Application in Microgrids

Zheng Zeng, *Student Member, IEEE*, Huan Yang, *Member, IEEE*, Shengqing Tang, and Rongxiang Zhao

***Abstract*—Multifunctional grid-tied inverters (MFGTIs) have been paid much attention to handle the commonly concerned power quality issues of the microgrids. An MFGTI can not only interface the renewable energy resource into the utility grid, but also can compensate the harmonic and reactive current in the microgrid as an auxiliary service. However, the apparent capacity of an MFGTI for power quality compensation is limited. Therefore, how to enhance the power quality of the microgrid by optimal utilization of the limited and valuable capacity becomes a technical challenge. In this paper, two optimal control objectives of MFGTIs are presented based on a comprehensive power quality evaluation algorithm by means of analytic hierarchy process theory. One objective aims to obtain the expected power quality using minimal apparent capacity of the MFGTI. Another objective focuses on enhancing the power quality as well as possible in the given available apparent capacity condition. The two proposed strategies are compared in performance, and the paper also discusses how to use them in practice for the best performance. Experimental results performed on a microgrid in the laboratory confirm the validation and feasibility of the proposed optimal control strategies.**

***Index Terms*—Analytic hierarchy process (AHP), comprehensive power quality evaluation, microgrid, multifunctional grid-tied inverter (MFGTI), objective-oriented optimal control strategy, power quality enhancement.**

I. Introduction

In order to interface the stochastic and intermittent renewable energy resources (RERs) into the utility network, microgrids are regarded as a potential solution, and these have attracted considerable attention recently [1]. Many microgrid demonstrations integrated with RERs, energy storage devices, local loads, protective and supervisory units are described in [2] and [3]. Nowadays, microgrids are a focus of research worldwide and are expected to play an important role in future electric network due to their desirable features. First, microgrids can be viewed as model citizens and/or virtual power plants to suppress the power fluctuation of RERs and make the RERs much more schedulable [4]. Second, the microgrids can also improve the stability of utility and inject proper active and/or reactive power into utility in the conditions of utility failures [5]. Furthermore, because of the flexible operation modes of the microgrids, such as grid-tied mode and islanded mode, the microgrids can effectively enhance the operation, control, dispatch, and the black-start of utility. Finally, the microgrids also can customize the power quality and provide flexible power supply to local loads [6].

However, the power quality requirement is always challenging the secure, stable, effective, and economic operation of microgrids. First, the parallel and/or series harmonic resonances may result in undesired trips of grid-tied inverters, and may even lead to some cascading failures [7], [8]. Second, the harmonic and reactive current flowing across the microgrid will cause extra power loss and lower the usage capacity of lines and loads. Particularly, the harmonic can cause vibration and noise of electric machines and transformers [9]. Finally, poor power quality will lead to poor on-grid electricity price in a power quality sensitive market in the future [10].

It is obvious that the power quality of microgrids is a key issue for their effective and economic operation. Therefore, the power quality issue of microgrids is drawing more and more attention. Recently, the multifunctional grid-tied inverter (MFGTI) has been considered as a solution with high cost-effectiveness [11]–[13]. The so-called MFGTI is an advanced grid-tied inverter which can not only interface RERs into utility, but also enhance the power quality at its grid-tied point [14]–[19]. On one hand, the grid-tied inverters have the same power conversion topologies as the ones of power quality conditioners, such as active power filters, static var generators, etc. On the other hand, in general, the capacity of a grid-tied inverter is larger than that of the installed photovoltaic arrays and/or wind turbines. Thus, it can adapt the stochastic and intermittent features of solar irradiation and/or wind speed. Additionally, the grid-tied inverters cannot always operate at their nominal capacity points. Thus, the surplus capacity of a grid-tied inverter is available in most of its operation time. Therefore, the grid-tied inverters have the additional capacity that can be utilized to enhance the power quality at their grid-tied points, in such a way that no extra power quality conditioner may be needed in an inverter-dominated microgrid. Nevertheless, the power quality enhancement is just the auxiliary functionality of an MFGTI. So the capacity of an MFGTI for power quality enhancement is limited, and most of its capacity is utilized to interface RERs

Manuscript received November 26, 2013; revised February 18, 2014; accepted March 25, 2014. Date of publication April 2, 2014; date of current version October 15, 2014. This work was supported in part by the National High Technology Research and Development Program of China (863 Program) under Grant 2011AA050204, in part by the National Natural Science Foundation of China under Grant 50907060, and in part by the China Postdoctoral Science Foundation under Grant 20090451438. Recommended for publication by Associate Editor M. Liserre.

The authors are with the College of Electrical Engineering, Zhejiang University, Hangzhou 310027, China (e-mail: zengerzheng@zju.edu.cn; yanghuan@zju.edu.cn; sentry2004@126.com; rongxiang@zju.edu.cn).

Color versions of one or more of the figures in this paper are available online at http://ieeexplore.ieee.org.

Digital Object Identifier 10.1109/TPEL.2014.2314742

into utility. Therefore, it is challenging to well organize and optimal use the valuable margin capacity. On one hand, coordinated control of the multiple MFGTIs in a microgrid can be a good choice to share the power quality issues. By means of conductance and susceptance limitation, a coordinated control of multiple MFGTIs is presented and verified by experimental results in [20]. On the other hand, how to optimally use the limited capacity of an MFGTI to enhance the power quality of the microgrid according to certain given objectives is becoming an urgent necessity [21]–[23]. In [24], a multiobjective optimal compensation strategy is presented for 3H-bridge MFGTI application. In order to simultaneously improve power quality and satisfy the load power demand, based on the catastrophe decision theory, a quality comprehensive evaluation method is proposed in [24] to guide the optimal power quality conditioning of the MFGTI. However, the physical mechanism of the catastrophe-decision-based method is not clear, and this method is difficult to satisfy the constitution including more than four power quality indicators. Besides, the special 3H-bridge MFGTI in [24] is not a common used two-level converter, so the proposed optimal control is hard to be directly implemented in microgrids or distributed generation systems.

The main aim of this paper is to propose an optimal compensation strategy of MFGTIs according to the objectives based on a comprehensive power quality index (CPQI) model. This paper is organized as follows. In Section II, the configuration and mathematical model of the microgrid and MFGTI are introduced. Then, using the CPQI model based on analytic hierarchy process (AHP) theory, the optimal compensation strategies of the MFGTI are presented in Section III where an advanced algorithm is indicated for the reference generation of the MFGTI. Experimental results are depicted in Section IV to verify the validation and feasibility of the proposed control strategy. In Section V, some discussion on the comparative performances and the best usage situation of two proposed control strategies are included. Finally, conclusions are drawn in Section VI.

II. Configuration of the Microgrid and Mathematical Model of the MFGTI

The investigated microgrid demonstration is an ongoing development in Zhejiang University, as shown in Fig. 1. This is a typical hybrid microgrid including a 100-kW ac sub-microgrid and a 30-kW dc sub-microgrid. The ac sub-microgrid is mainly considered in this paper which consists of a 5-kW permanent magnet (PM) wind generator, a 5-kW direct drive PM wind power simulator, 3-kW photovoltaic (PV) arrays inverters, 30-kW grid-tied fuel cells, hybrid energy storage devices including 15-kW/14.2 kWh Li-ion battery units and 15-kW supercapacitor units to suppress the power fluctuation of the RERs, a controllable local load, and a feeder with 20-kW MFGTIs. Beside the fuel cell connected at bus B, other distributed generation units and local load are connected at distribution boxes (DB) of bus C in the test-bed room. Buses B and C are connected to 380-V/50-Hz three-phase three-wire distribution network by isolated transformers. The main devices of the microgrid are listed in Table I.

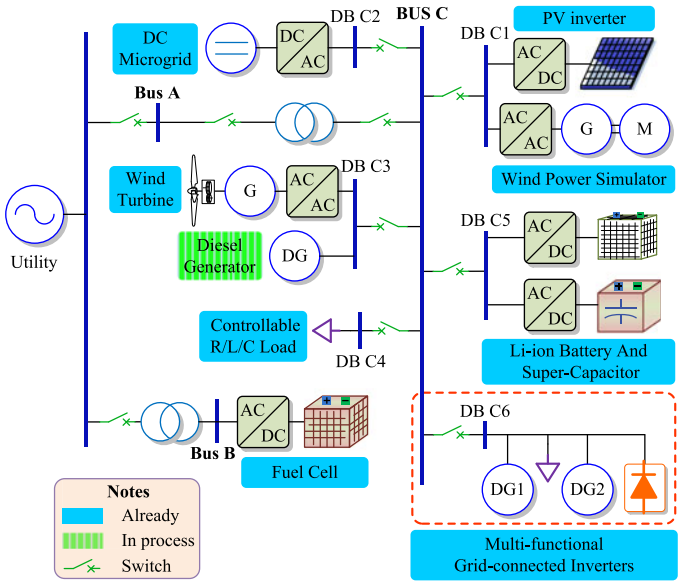

Fig. 1. Configuration of the microgrid demonstration system in Zhejiang University.

TABLE I
Main Devices of the AC Sub-Microgrid

Device	Type	Capacity	Notes
Wind generator	Source	5kW	Single-phase
PV arrays	Source	3kW	Thin-film,1kW per phase
Diesel Generator	Source	5kW	In process
Wind power simulator	Source	5kW	Direct drive PM generator
Fuel cell	Source	30kW	Hydrogen-Oxygen
Li-ion battery	Energy storage	15kW/14.2kWh	Hybrid energy storage units
Super-capacitor	Energy storage	15kW	
MFGTIs	Source	20kW	Power quality conditioning
Controllable load	Load	30kW/15kVar	Passive loads

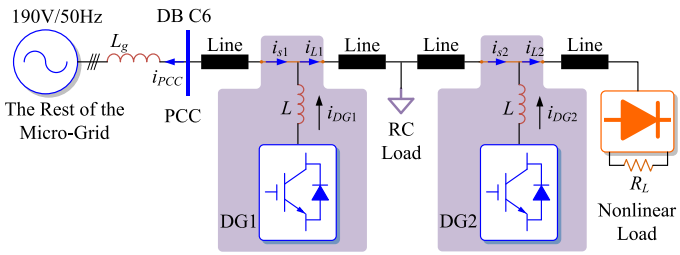

Fig. 2. Single-line schematic of the feeder DB C6.

The MFGTIs are connected at feeder DB C6 of the microgrid. Two identical 10-kVA distributed generators (DGs) via MFGTIs are considered together with some local loads. Additionally, the DB C6 can be considered as the point of common coupling (PCC) of the feeder. From the point of view of DB C6, other feeders and the utility network can be viewed as a set of ac sources with inner inductor L_g, so that the feeder can be simplified as shown in Fig. 2. Additionally, DG1 and DG2 both employ the two-level voltage source converter topology, and the detailed schematic is depicted in Fig. 3.

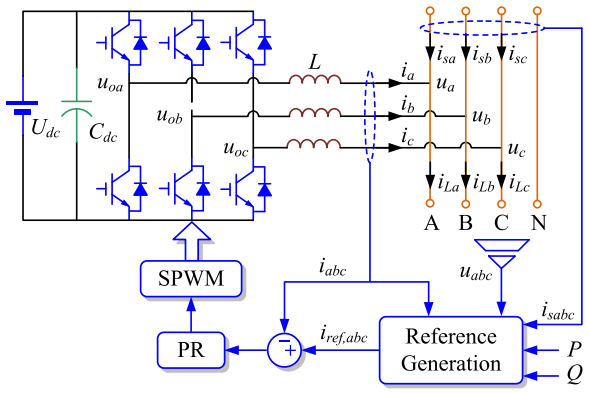

Fig. 3. Topology and the overview control strategy of the MFGTI.

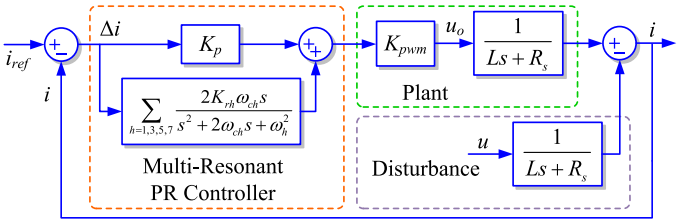

Fig. 4. Control block diagram of the MFGTI.

The dynamic response of the grid-tied current i_{abc} of the MFGTI, across the filter inductor L, can be expressed as

$$L\dot{i}_{abc} = u_{oabc} - u_{abc} - R_s i_{abc} \tag{1}$$

where R_s is the parasitic resistance of the inductor, u_{oabc} denotes the ac output voltage of the inverter, and u_{abc} represents the voltage at the point of inverter connection. Supposing the system is symmetrical, for arbitrary phase, the transfer functions between grid-tied current and voltage can be, respectively, expressed as

$$G_1 = I(s)/U_o(s) = 1/(Ls + R_s) \tag{2}$$

$$G_2 = I(s)/U(s) = -1/(Ls + R_s). \tag{3}$$

Furthermore, the block diagram of the grid-tied inverter can be depicted in Fig. 4.

From Fig. 3, it can be seen that each MFGTI module samples its output current i_{abc} and the upstream current i_{sabc} flowing over it. The algorithm to calculate reference current $i_{\mathrm{ref},abc}$ will be presented in Section III. The output current i_{abc} is the feedback for tracking its reference values $i_{\mathrm{ref},abc}$, as shown in Fig. 4. With the aid of the multiresonant proportional resonant (PR) controller, the trigger pulses of the IGBTs can be obtained by the sinusoidal pulse-width modulation. To avoid the failure of decoupling control in synchronous rotating *dq* frame, which is caused by the perturbation of inductance, the current-tracking is realized in the natural *abc* frame using PR controller. The multiresonant PR controller associated with fundamental, third-, fifth-, and seventh-order harmonic components [25]–[27] can be expressed as

$$G_{PR}(s) = \sum_{h=1,3,5,7} \frac{2K_{rh}\omega_{ch}s}{s^2 + 2\omega_{ch}s + \omega_h^2} \tag{4}$$

where ω_1 and ω_h are the natural angular frequencies of the fundamental and hth-order harmonic resonant terms, ω_{c1} and ω_{ch} are the cut-off frequencies of these terms, K_p and K_{rh} $(h = 1, 3, 5, 7)$ are the proportional and resonant integral gains of the PR controller.

III. Objective-Oriented Optimal Compensation of the MFGTI

A. Algorithm to Generate the Reference Current

The approaches of traditional power quality conditioners consider the harmonic and reactive current has the same weight without objective-based compensation. Unlike these conditioners, to optimally utilize the limited capacity of an MFGTI, the objective-oriented optimal compensation strategy is presented in this paper. Besides, the harmonic and reactive current components in the microgrid are distinguished using the different contributing weights, according to the proposed CPQI model based on the AHP theory. The algorithm to generate the reference current of a MFGTI is depicted in Fig. 5. The reference current $i_{\mathrm{ref},abc}$ consists of two parts [11], [12], [16]. One is used for power generation tracking to interface the RERs into utility and the other part is utilized to optimally compensate the harmonic and reactive current in the microgrid based on the objective model.

To generate the reference current, a nonphase-locked-loop (non-PLL) approach is employed to make the algorithm easy to be implemented on a DSP control board. In Fig. 5, $\theta = 2\pi ft$ is the angle corresponding to the fundamental line-frequency f of the utility network, and $\boldsymbol{T}_{3s/2s}$ represents the Clarke transformation

$$\boldsymbol{T}_{3s/2s} = \sqrt{\frac{2}{3}} \begin{bmatrix} 1 & -1/2 & -1/2 \\ 0 & -\sqrt{3}/2 & \sqrt{3}/2 \end{bmatrix} \tag{5}$$

whose inverse transformation satisfies $\boldsymbol{T}_{2s/3s} = \boldsymbol{T}_{3s/2s}^T$. The symbol $\boldsymbol{T}_{2s/2r}$ in Fig. 5 denotes the rotating transformation

$$\boldsymbol{T}_{2s/2r} = \begin{bmatrix} \cos\theta & \sin\theta \\ -\sin\theta & \cos\theta \end{bmatrix} \tag{6}$$

whose inverse transformation satisfies $\boldsymbol{T}_{2r/2s} = \boldsymbol{T}_{2s/2r}^T = \boldsymbol{T}_{2s/2r}^{-1}$. The matrix $\boldsymbol{T}_1$ in Fig. 5 is implemented to generate the reference current i_{gdq} for power generation in synchronous rotating *dq* frame, which can be expressed as

$$\begin{bmatrix} i_{gd} \\ i_{gq} \end{bmatrix} = \boldsymbol{T}_1 \begin{bmatrix} \bar{u}_d \\ \bar{u}_q \end{bmatrix} = \frac{1}{\bar{u}_d^2 + \bar{u}_q^2} \begin{bmatrix} P & Q \\ -Q & P \end{bmatrix} \begin{bmatrix} \bar{u}_d \\ \bar{u}_q \end{bmatrix} \tag{7}$$

where P and Q are the reference active and reactive power of the RERs, $\bar{u}_{dq}$ stand for the utility voltage in *dq* frame after low-pass filtering.

The transformation matrix $\boldsymbol{T}_2$ in Fig. 5 is employed to separate the fundamental active and reactive components, i_{pdq} and i_{qdq}, from the equivalent load current $(i_{Labc} = i_{sabc} + i_{abc})$ in *dq* frame i_{Ldq}, which can be written as

$$\begin{bmatrix} i_{pd} \\ i_{pq} \end{bmatrix} = \frac{\bar{u}_d \bar{i}_{Ld} + \bar{u}_q \bar{i}_{Lq}}{\bar{u}_d^2 + \bar{u}_q^2} \begin{bmatrix} 1 & 0 \\ 0 & 1 \end{bmatrix} \begin{bmatrix} \bar{u}_d \\ \bar{u}_q \end{bmatrix} \tag{8}$$

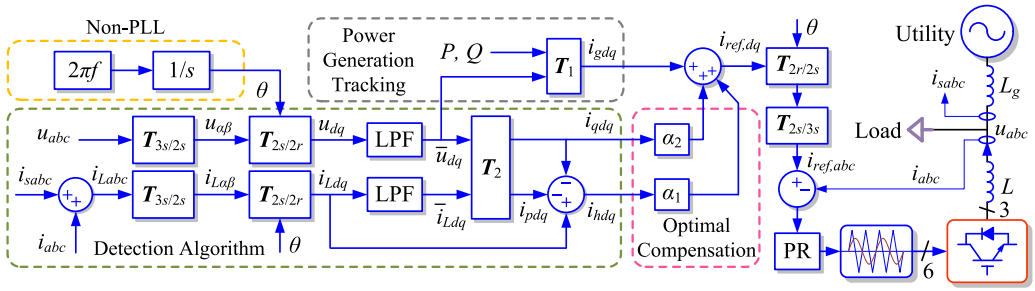

Fig. 5. Algorithm for the MFGTI to generate the reference current.

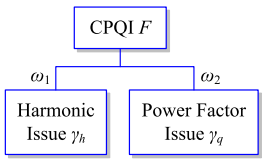

Fig. 6. Model of comprehensive power quality evaluation.

$$\begin{bmatrix} i_{qd} \\ i_{qq} \end{bmatrix} = \frac{\bar{u}_q \bar{i}_{Ld} - \bar{u}_d \bar{i}_{Lq}}{\bar{u}_d^2 + \bar{u}_q^2} \begin{bmatrix} 0 & 1 \\ -1 & 0 \end{bmatrix} \begin{bmatrix} \bar{u}_d \\ \bar{u}_q \end{bmatrix}. \tag{9}$$

Then, the harmonic current in *dq* frame can be expressed as

$$i_{hdq} = i_{Ldq} - i_{pdq} - i_{qdq}. \tag{10}$$

In summary, the detected harmonic and reactive equivalent load current in *dq* frame is multiplied by the optimal compensation coefficients, namely, α_1 and α_2, and added to the reference current for power generation i_{gdq} to form the reference current in *dq* frame. With the help of the inverse transformations, the reference current in *abc* frame can be derived. The optimal compensation coefficients can be obtained in the following subsection.

B. Model and Solution of the Objective-Oriented Optimal Compensation Strategy

The CPQI model to evaluate the power quality at PCC of the microgrid can be depicted in Fig. 6 using the AHP theory. According to the AHP-based CPQI model, the total harmonic distortion (THD) and power factor (PF) of the current flowing across the PCC contribute the CPQI F with different weights ω_1 and ω_2. If the harmonic issue of microgrid is somewhat more important than reactive power issue, according to the AHP theory presented by T. L. Saaty etc. [28], the comparison matrix can be chosen as

$$\boldsymbol{C} = \begin{bmatrix} 1 & 3 \\ 1/3 & 1 \end{bmatrix}. \tag{11}$$

The eigenvalues and eigenvectors of $\boldsymbol{C}$ can be derived, and the coincident justice can be written as

$$CI = (\lambda_{\max} - n)/(n-1) \tag{12}$$

where $\lambda_{\max} = 2$ is the maximum eigenvalue of $\boldsymbol{C}$, and $n = 2$ is the order of $\boldsymbol{C}$. It can be found that $CI = 0$, so the coincident judgment is passed according to the AHP theory. Normalized the eigenvector corresponding to the maximum eigenvalue $\lambda_{\max}$, the weights of the CPQI model can be obtained as $\boldsymbol{\omega} = (\omega_1, \omega_2) = (0.75, 0.25)$. According to the CPQI model in Fig. 6, the CPQI can be expressed as $F = \omega_1\gamma_h + \omega_2\gamma_q$, where γ_h and γ_q are the harmonic and reactive coefficients of PCC current will be defined in the following part.

In the following parts, two different objectives are proposed based on the aforementioned CPQI model for the optimal compensation of the MFGTI.

1) Objective I: Employing Minimum Capacity to Maximally Enhance the Power Quality of the Microgrid: 1. *Objective function:* In such objective, the capacity of the MFGTI employed for power quality compensation can be expressed as

$$S = \sqrt{S_h^2 + S_q^2} = 3U\sqrt{(\alpha_1 I_{h0})^2 + (\alpha_2 I_{q0})^2} \tag{13}$$

where S_h and S_q are the capacity of the MFGTI employed for harmonic and reactive compensation, respectively, U is the root-mean-square (RMS) value of the utility phase-to-ground voltage, I_{h0} and I_{q0} are the RMS values of the harmonic and reactive current before the MFGTI starts to compensate, α_1 and α_2 are the optimal compensation coefficients of the MFGTI for power quality enhancement. Therefore, the optimal compensation objective I can be chosen as

$$\min \quad F_1 = S^2/(9U^2) = \alpha_1^2 I_{h0}^2 + \alpha_2^2 I_{q0}^2 \tag{14}$$

where

$$\begin{cases} I_{h0} = \gamma_{h0} I_1 \\ I_{q0} = \gamma_{q0} I_1 \end{cases} \tag{15}$$

where γ_{h0} and γ_{q0} are the initial harmonic and reactive coefficients of PCC current i_{PCC} before the compensation of the MFGTI, respectively. γ_{h0} can be chosen as the THD, while γ_{q0} is defined as the ratio between reactive and fundamental components of the current, even as the RMS value ratio between the reactive current I_q and fundamental current I_1, which can be expressed as

$$\gamma_q = Q/(3UI_1) = (3UI_q)/(3UI_1) = I_q/I_1. \tag{16}$$

2. Supposing the harmonic and reactive coefficients of the PCC current are γ_h and γ_q after the compensation of the MFGTI, the CPQI in such a condition can be written as

$$\omega_1\gamma_h + \omega_2\gamma_q = A \tag{17}$$

where A is the set target and is a constant. The target CPQI A of the microgrid at PCC should be set according to the power quality standards of the utility or the schedule of the utility. On one hand, according to the power quality regulations in

the utility, the THD and PF should be controlled in the proper ranges, such as THD $< 5\%$ and PF > 0.98. Therefore, the target A can be directly calculated according to the power quality regulations in such conditions. On the other hand, as indicated in [29], the grid-tied inverters should be scheduled to participate in many services of the utility, such as reactive power supporting, power quality enhancement, and so on. In such conditions, to support the power quality enhancement and reactive stability of the utility, the CPQI A can be given by the distribution network operator and guides the MFGTI to generate the desired harmonic and reactive power into utility. It should be noted that a smaller A represents better power quality level of the microgrid. Therefore, the set CPQI A should be smaller than the one σ before the compensation of the MFGTI which can be expressed as

$$\sigma = \omega_1 \gamma_{h0} + \omega_2 \gamma_{q0}. \tag{18}$$

Apparently, if all the harmonic and reactive current components are compensated, γ_h and γ_q should be zeroes, so that CPQI $F = A = 0$.

Generally, the load power demand and the power generation of DGs are constant in a time interval, the RMS value of the fundamental current is approximately the same before and after compensation of the MFGTI. For convenience, I_1 is considered as constant. In ideal conditions, the harmonic and reactive coefficients, after the compensation of the MFGTI, can be expressed as

$$\begin{cases} \gamma_h = (1-\alpha_1)\gamma_{h0} \\ \gamma_q = (1-\alpha_2)\gamma_{q0} \end{cases} \tag{19}$$

where α_1 and α_2 are the ratios of compensated harmonic and reactive current components in the microgrid. Thus, the remaining harmonic and reactive coefficients after the MFGTI starts to compensate should be $(1-\alpha_1)$ and $(1-\alpha_2)$ of the initial ones, respectively.

3. Lagrange's function to solve the objective model can be written as

$$L_1 = \alpha_1^2 I_{h0}^2 + \alpha_2^2 I_{q0}^2 + \lambda_1(\omega_1\gamma_h + \omega_2\gamma_q - A) \tag{20}$$

where λ_1 is the Lagrange multiplier of objective I, in unit I^2/CPQI. It should be noted that, if no power quality compensation action is taken, the Lagrange's function meets $L_1 = 0$ in the conditions of $\alpha_1 = \alpha_2 = 0$ and $A = \sigma$. On the contrary, if all the harmonic and reactive current is compensated, L_1 is $I_{h0}^2 + I_{q0}^2$ in the conditions of $\alpha_1 = \alpha_2 = 1$ and $A = 0$. Thus, the value of Lagrange's function L_1 is within the interval [0, $I_{h0}^2 + I_{q0}^2$]. According to (20), it can be found that

$$\begin{cases} \partial L_1/\partial\alpha_1 = 2\alpha_1(\gamma_{h0}I_1)^2 - \lambda_1\gamma_{h0}\omega_1 = 0 \\ \partial L_1/\partial\alpha_2 = 2\alpha_2(\gamma_{q0}I_1)^2 - \lambda_1\gamma_{q0}\omega_2 = 0 \\ \partial L_1/\partial\lambda_1 = \omega_1\gamma_h + \omega_2\gamma_q - A = 0. \end{cases} \tag{21}$$

Therefore, the solutions of the optimal model can be written as

$$\begin{cases} \alpha_1 = (\sigma - A)\omega_1/\left[(\omega_1^2+\omega_2^2)\gamma_{h0}\right] \\ \alpha_2 = (\sigma - A)\omega_2/\left[(\omega_1^2+\omega_2^2)\gamma_{q0}\right] \\ \lambda_1 = 2(\sigma - A)I_1^2/(\omega_1^2+\omega_2^2). \end{cases} \tag{22}$$

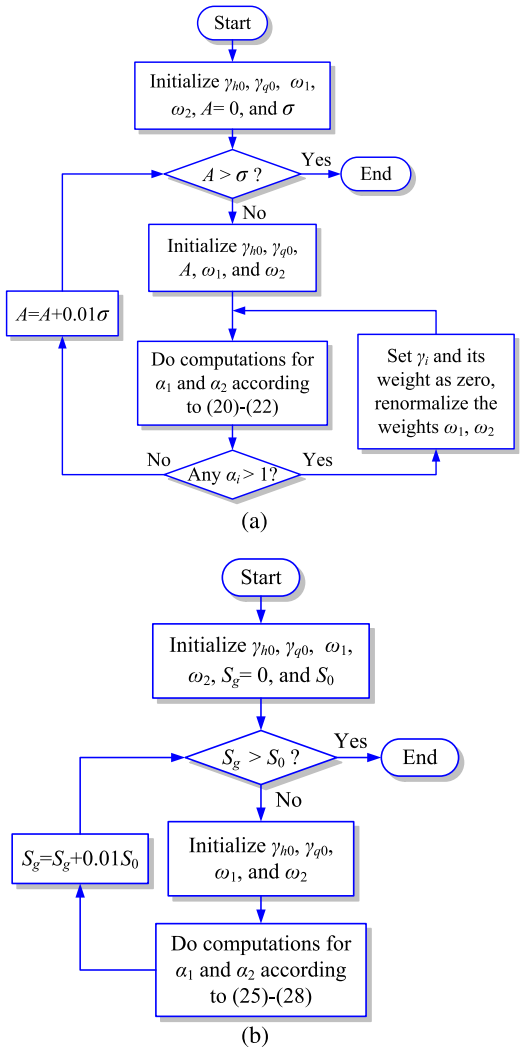

Fig. 7. Flowcharts to solve the optimal compensation model of the MFGTI according to (a) objective I for $A \in [0, \sigma]$ and (b) objective II for $S_g \in [0, S_0]$.

It can be seen that the optimal compensation coefficients α_1 and α_2 are related to the weights ω_1 and ω_2, so the approaches to get the CPQI may affect the optimal compensation strategy. Thus, except for AHP approach, some other power quality comprehensive evaluation approaches can be employed for the objective-oriented compensation of MFGTI and may get some different results [24].

According to the analysis mentioned earlier, flowchart to obtain the optimal compensation coefficients of the objective I model can be demonstrated in Fig. 7(a). It should be noted that, by means of energy management system (EMS), this optimal calculation can be completed in the tertiary control of a hierarchical controlled microgrid [30]. Then, according to the dynamic generation and load levels, the EMS downloads the optimal coefficients α_1 and α_2 to the MFGTI controller in real time. In Fig. 7(a), as aforementioned, the parameters γ_{h0} and γ_{q0} are the harmonic and reactive coefficients of PCC current, respectively, before the MFGTI compensates the power quality issues. Additionally, parameters ω_1 and ω_2 are weights of the power quality indicators and can be set by the mentioned

AHP-based CPQI model. Thus, σ is the CPQI in the condition of γ_{h0}, γ_{q0}, ω_1, and ω_2, as shown in (18). For any given CPQI A, it can be found an optimal solution (α_1, α_2) according to the flowchart in Fig. 7(a). When the given CPQI A varies in the interval [0, σ], the solution set of optimal compensation coefficients for objective I application can be obtained. It should be noted that when the compensation coefficient of one power quality indictor larger than 1, this power quality indictor can be considered to be eliminated in the AHP-based CPQI model. Then, the algorithm repeats the calculation in (20)–(22) and calculates the compensation coefficient of the left power quality indictor.

2) Objective II: Minimizing the CPQI in the Condition of Given Capacity for Power Quality Enhancement: According to the comprehensive power quality evaluation model, the optimal objective II can be expressed as

$$\min \quad F_2 = \omega_1\gamma_h + \omega_2\gamma_q. \tag{23}$$

1. Supposing the given capacity of the MFGTI for power quality enhancement is set as S_g, it can be written as

$$S_g = 3U\sqrt{\alpha_1^2 I_{h0}^2 + \alpha_2^2 I_{q0}^2}. \tag{24}$$

2. According to (23) and (24), the Lagrange's function can be chosen as

$$L_2 = \omega_1\gamma_h + \omega_2\gamma_q + \lambda_2\left(3U\sqrt{\alpha_1^2 I_{h0}^2 + \alpha_2^2 I_{q0}^2} - S_g\right) \tag{25}$$

where S_g is the available margin capacity of the MFGTI, λ_2 is the Lagrange multiplier of objective II, in unit CPQI/S. Similar with the results of objective I, if no power quality enhancement is employed, there is $L_2 = \sigma$ in the condition of $\alpha_1 = \alpha_2 = 0$ and $S_g = 0$. On the contrary, if all the harmonic and reactive current are totally compensated, then there is $L_2 = 0$ in the condition of $\alpha_1 = \alpha_2 = 1$ and S_g=$S_m = 3U\sqrt{I_{h0}^2 + I_{q0}^2}$, where S_m is the capacity of harmonic and reactive current. Therefore, L_2 is within [0, σ]. According to (25), it can be derived that

$$\begin{cases} \partial L_2/\partial\alpha_1 = -\omega_1\gamma_{h0} + 3\lambda_2 U\alpha_1 I_{h0}^2 \Big/ \sqrt{\alpha_1^2 I_{h0}^2 + \alpha_2^2 I_{q0}^2} = 0 \\ \partial L_2/\partial\alpha_2 = -\omega_2\gamma_{q0} + 3\lambda_2 U\alpha_2 I_{q0}^2 \Big/ \sqrt{\alpha_1^2 I_{h0}^2 + \alpha_2^2 I_{q0}^2} = 0 \\ \partial L_2/\partial\lambda_2 = \alpha_1^2 I_{h0}^2 + \alpha_2^2 I_{q0}^2 - S_g^2/(9U^2) = 0. \end{cases} \tag{26}$$

Then,

$$\begin{cases} \alpha_1 = \omega_1\gamma_{h0} S_g I_{q0} \Big/ (3UI_{h0}\sqrt{(\omega_1\gamma_{h0} I_{q0})^2 + (\omega_2\gamma_{q0} I_{h0})^2}) \\ \alpha_2 = \omega_2\gamma_{q0} S_g I_{h0} \Big/ (3UI_{q0}\sqrt{(\omega_1\gamma_{h0} I_{q0})^2 + (\omega_2\gamma_{q0} I_{h0})^2}) \\ \lambda_2 = \sqrt{(\omega_1\gamma_{h0} I_{q0})^2 + (\omega_2\gamma_{q0} I_{h0})^2} \Big/ (3UI_{h0} I_{q0}). \end{cases} \tag{27}$$

Unlike the situations mentioned before in the part about objective I, when the optimal compensation coefficient of one power quality indictor approaches 1, the calculation for another indictor should be paid special attention, and the model in (23)–(27) should be rebuilt. For instance, if the optimal coefficient of harmonic component α_1 reaches at 1 first, the coefficients α_2 and λ_2 should be calculated as

$$\begin{cases} \alpha_2 = \sqrt{S_g^2 - (3UI_1\gamma_{h0})^2} \Big/ (3UI_1\gamma_{q0}) \\ \lambda_2 = \sqrt{\alpha_2^2(\gamma_{q0} I_1)^2 + (\gamma_{h0} I_1)^2} \Big/ (3U\alpha_2\gamma_{q0} I_1^2). \end{cases} \tag{28}$$

According to (27) and (28), the flowchart to obtain the optimal compensation coefficient can be depicted in Fig. 7(b). It can be seen that, for any given S_g in the interval [0, S_0], the proposed model can achieve an optimal solution (α_1, α_2) for objective II application.

TABLE II
IMPORTANT PARAMETERS OF THE MFGTI PROTOTYPE

U_{dc} (V)	L (mH)	R_s (Ω)	C_{dc} (μF)	R_L (Ω)	L_g (mH)
350	0.5	0.05	4400	20	3

IV. EXPERIMENTAL VALIDATIONS

To confirm the validation and feasibility of the proposed control strategies, the experimental prototype in the ongoing microgrid demonstration is built. In the feeder DB C6 of the microgrid, two identical 10-kVA MFGTIs are integrated as shown in Figs. 1 and 2. DSP TMS320F2812 is utilized and the switching frequency of IGBTs is set to 10 kHz. Besides, local loads (a capacitive and resistive load 1000 μF and 10 Ω and a diode rectifier load with $R_L = 20\ \Omega$) are also included in the feeder DB C6 as shown in Fig. 2. The nominal line-to-line peak-voltage and line-frequency of the utility network are 190 V and 50 Hz, respectively. The important parameters of the prototype are listed in Table II, and the parameters of the PR controller are chosen as $K_p = 2.5$, $K_{rh} = 20$ and $\omega_{c1} = \omega_{ch} = 5$ rad/s.

A. Performance of MFGTI on Power Generation

To verify the performance of the designed multiresonant PR controller on current-tracking for power generation of RERs, the steady-state and dynamic responses of the MFGTI have been checked, in the condition of that its reference active and reactive power steps from 4 to 6 kW, and from 2 to –2 kVar, respectively. The instantaneous output grid-tied current and power curves of the MFGTI are shown in Fig. 8. From Fig. 8, it can be found that, the designed controller has good performances on grid-tied current-tracking. The steady-state error of the current-tracking is approximate 1A.

Fig. 9 depicts the steady-state performance of the MFGTI on the PF, THD, and the efficiency. It can be seen that when the reference active power is larger than 3 kW, the THD will drop below 5%. Due to the zero-phase-shift feature of the multiresonant PR controller, the PF of the grid-tied current of the MFGTI can be maintained at a very high level. Additionally, the efficiency of the MFGTI will increase when the reference active power increases.

B. Performance of the MFGTI on Power Quality Enhancement

In Fig. 2, just DG1 works as an MFGTI, and the reference active/reactive power of DG1 and DG2 for power generation

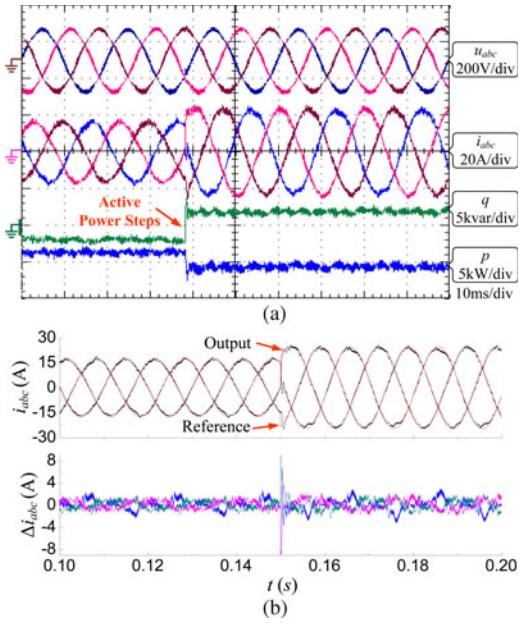

Fig. 8. Experimental results of the designed PR controller on current tracking. (a) Measured instantaneous waveforms, and (b) comparison of the reference and actual output grid-tied current.

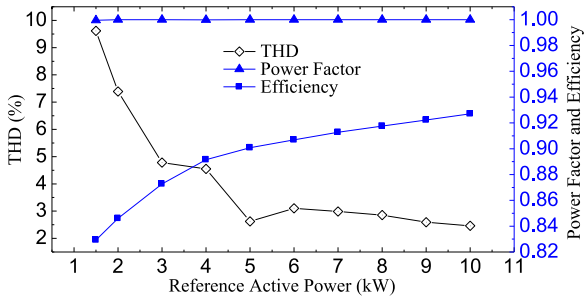

Fig. 9. Performance of the MFGTI in different reference active power conditions.

are 7 kW/0Var and 8 kW/0Var, respectively. The instantaneous current and power at PCC, as indicated in Fig. 2, are demonstrated in Fig. 10, when DG1 transfers from no compensation ($\alpha_1 = \alpha_2 = 0$) to full compensation ($\alpha_1 = \alpha_2 = 1$).

From Fig. 10(a) and (b), it can be found that, before DG1 starts to make power quality compensation, the THD of utility voltage and grid-tied current at PCC are 4.24% and 13.16%, respectively, while the PF of the grid-tied current is 0.9744. In this case, $\gamma_{h0} = 13.16\%$, $\gamma_{q0} \approx \sin[\text{acos}(0.9744)] = 0.2248$, the CPQI is $\sigma = \omega_1\gamma_{h0} + \omega_2\gamma_{q0} = 0.1549$ in the condition of $\omega_1 = 0.75$ and $\omega_2 = 0.25$. After DG1 starts power quality compensating, the THD of utility voltage is 4.21%, and the THD and PF of the grid-tied current at PCC are 6.43% and 0.9999, respectively. It is worth noting that the MFGTI or DG1 can greatly enhance the power quality at PCC. On one hand, the PF is hugely increased, while the instantaneous reactive power of grid-tied current at PCC is controlled to zero. On the other hand, the grid-tied current is much more sinusoidal, and the power fluctuation due to the harmonic current components can be effectively immunized. However, in the full compensation ($\alpha_1 = \alpha_2 = 1$) condition, the capacity of the MFGTI employed

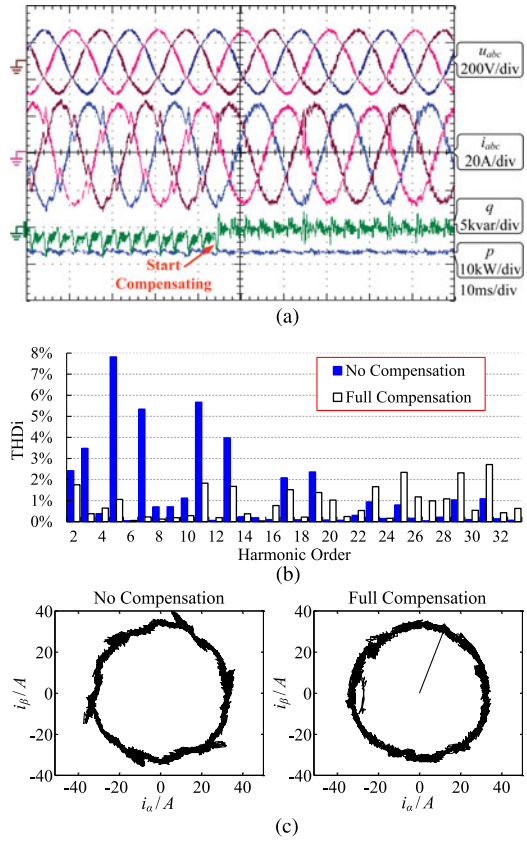

Fig. 10. Experimental results of the MFGTI from no compensation ($\alpha_1 = \alpha_2 = 0$) to full compensation ($\alpha_1 = \alpha_2 = 1$). (a) Waveforms at PCC, (b) harmonic distribution of the grid-tied current at PCC, and (c) phasor diagram of the current before and after DG1 starts to fully compensate.

for power quality enhancement is nearly 1.711 kVA, that is to say that 17.11% of its nominal capacity (10 kVA) is utilized to compensate for the power quality issues. It should be noted that the power quality enhancement is just the auxiliary functionality of an MFGTI, and most of its capacity should be utilized to interface the RERs into utility. So, much capacity of an MFGTI is employed for power quality enhancement is not always ideal and not practical in some cases. Therefore, it is obviously necessary to optimally dispatch the limited and valuable capacity to enhance the power quality of the microgrid.

From the phasor diagram of the grid-tied current at PCC in stationary $\alpha\beta$ frame as shown in Fig. 10(c), it can be observed that the grid-tied current has six peaks in the $\alpha\beta$ frame, due to the commutation of the diodes of the nonlinear load every 60°. On the contrary, after DG1 starts to compensation and injects harmonic current into the microgrid, the grid-tied current in the phasor diagram much approximates a standard circle. It can be concluded that the harmonic current in the microgrid is well compensated by the MFGTI or DG1.

C. Performance of the MFGTI on the Objective-Oriented Optimal Compensation

First, take the case of objective I into consideration, to obtain the set CPQI after compensation and employ the minimum capacity of the MFGTI, using the mathematical model in

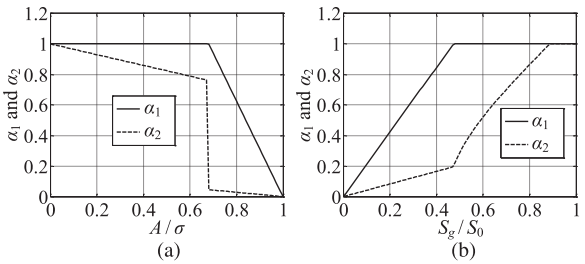

Fig. 11. Solutions the optimal compensation model in (a) objective I and (b) objective II conditions.

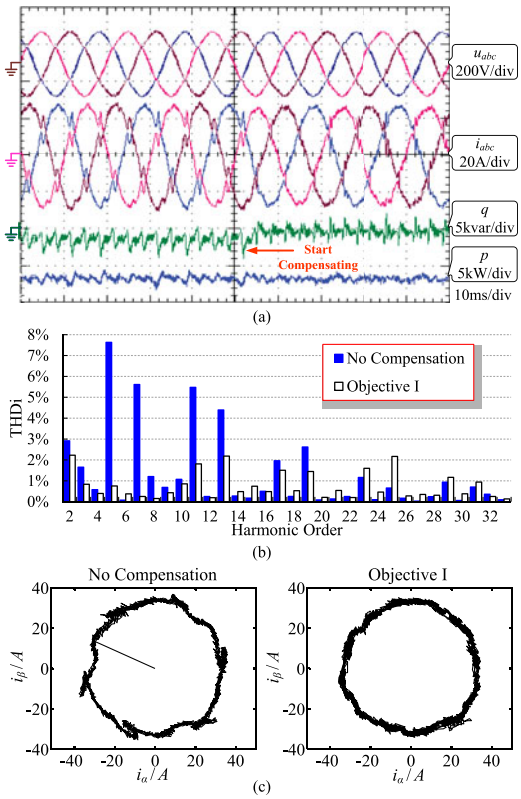

Fig. 12. Experimental dynamic responses of the MFGTI from no compensation to optimal compensation based on objective I ($\alpha_1 = 1$, $\alpha_2 = 0.8242$). (a) Waveforms of instantaneous current and power, (b) harmonic distribution of grid-tied current at PCC, and (c) phasor diagram of grid-tied current at PCC.

Section III, flowchart in Fig. 7(a), and the experimental results in Fig. 10, the optimal compensation coefficients in such condition can be derived as depicted in Fig. 11(a) where $\gamma_{h0} = 13.16\%$, $\gamma_{q0} = 0.2248$, and $\sigma = 0.1549$ as mentioned in Section IV-B.

For instance, to customize the CPQI as half of σ, namely, $A = 0.5\sigma = 0.0775$, from Fig. 11(a), the optimal compensation coefficients can be chosen as $\alpha_1 = 1$ and $\alpha_2 = 0.8242$. The dynamic responses of the MFGTI from no compensation to the optimal compensation using objective I are indicated in Fig. 12. The results show that, the THD of the utility voltage before compensation of DG1 is 4.05%, and the THD and PF of grid-tied current are 12.97% and 0.9762. After DG1 starts power quality compensating, the THD of the utility voltage is 3.88%, and the THD and PF of grid-tied current at PCC are 6.11% and 0.9990, respectively. Practically, the CPQI of PCC decreases from 0.155 to 0.057; on the contrary, the employed capacity of the MFGTI is 1.635 kVA. It can be seen that, according to objective I, the MFGTI compensates the reactive current in the microgrid. Based on the aforementioned CPQI model, the harmonic issue has much bigger weight than the reactive one, so as that the MFGTI paid much more effort to compensate the harmonic issue in the microgrid. Similarly, the phasor diagram of the grid-tied current at PCC is depicted in Fig. 12(c). Compared with the current in phasor diagram before compensation of DG1, the one after DG1 starts to compensation approximates a standard circle much better.

In the following part, the optimal compensation operation of the MFGTI in objective II mode will be explained in detailed. According to objective II, the MFGTI should enhance the power quality at PCC as good as possible using the given capacity. According to the objective model and the solution approach in Section III, the solution in objective II model can be depicted in Fig. 11(b) where $\gamma_{h0} = 13.16\%$, $\gamma_{q0} = 0.2248$, and $S_0 = 2$ kVA.

From Fig. 11(b), it can be found that, the desired capacity of an MFGTI is $S_g = 0.9 \times S_0 = 0.9 \times 2$ kVA $= 1.8$ kVA to full compensate all the harmonic and reactive current in the microgrid. For example, if the set capacity of the MFGTI for power quality enhancement is half of the one for full compensation, namely, 0.9 kVA, the optimal compensation coefficients should be $\alpha_1 = 0.5106$ and $\alpha_2 = 0.4327$ according to the solution of objective II in Fig. 11(b). Noted that the weights of the harmonic and reactive issues for CPQI are not linear, thus their weights are not 0.5. Fig. 13 depicts the dynamic responses when DG1 transfers from no compensation model to objective II mode. Before DG1 starts to compensate, the THD of the utility voltage is 4.21%, the THD and PF of the grid-tied current are 12.97% and 0.9774, respectively. After DG1 starts to compensate, the THD of utility voltage is 3.93%, as well as the THD and PF of the grid-tied current are 6.78% and 0.9919, respectively. The CPQI decreases from 0.1501 to 0.08447, after DG1 transfers to objective II model, while the actual employed capacity of DG1 is 1.33 kVA. Due to the error of current-tracking controller shown in Fig. 8, the actual employed capacity is larger than the set one 0.9 kVA. But it is smaller than the one of objective I mode all the same, while the CPQI of objective II is larger than the one of objective I.

V. Discussions

As mentioned earlier, two optimal objective-oriented control strategies of the MFGTI are presented for the microgrid application. However, the relationship and the best usage situations of the two control objectives should be discussed. The two identical objectives aforementioned can be regarded as a universal multiobjective model, which consists of two minimal objectives and a constraint. It can be expressed as

$$\begin{cases} \min \quad S = \sqrt{\alpha_1^2 I_{h0}^2 + \alpha_2^2 I_{q0}^2} \\ \min \quad F = \omega_1 \gamma_h + \omega_2 \gamma_q \\ \text{cons.} \quad 0 \le \alpha_i \le 1 \ (i = 1, 2). \end{cases} \tag{29}$$

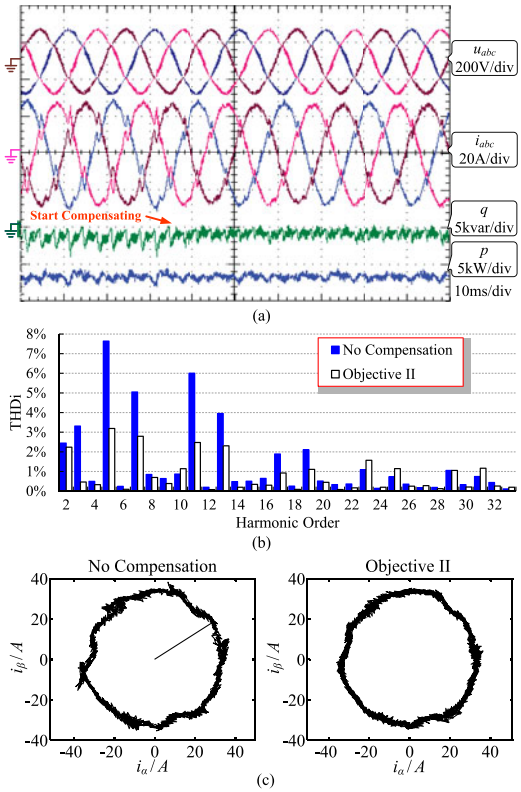

Fig. 13. Experimental dynamic responses of the MFGTI from no compensation to optimal compensation based on objective II ($\alpha_1 = 0.5106, \alpha_2 = 0.4327$). (a) Waveforms of the instantaneous current and power, (b) harmonic distribution of the grid-tied current, and (c) phasor diagram of the grid-tied current.

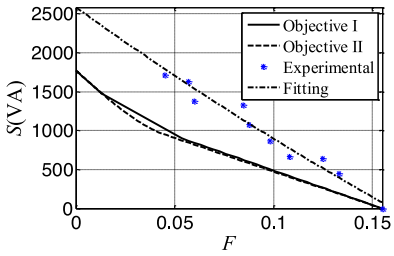

Fig. 14. Simulation and experimental Pareto optimal solutions of the multiobjective model.

Fig. 14 indicates the Pareto optimal solutions of the multiobjective model in (29). It can be observed that the two identical objectives previously mentioned in Fig. 11 can obtain nearly the same results in the viewpoint of multiobjective optimization meaning.

To support the validity and benefits of the control strategy proposed, much more experimental results are measured with more sets of parameters as shown in Fig. 14. It can be seen that, for each F value, the compensation capacity in the experimental results is bigger than the one in theoretical Pareto optimal solutions, because the current-tracking controller in real world cannot achieve the zero-error performance accurately.

Additionally, since the converter ratings can be increased with relatively small cost compared to a new device or additional energy storage and distributed energy resources, it also needs to compare the two methods with increased power rating as a variable to determine the most cost-effective control strategy. In this paper, to quantify the performances of the two objectives on the increased power rating, a variable *dS/dF* is defined as the sensitivity of employed compensation capacity when the CPQI changes. As mentioned earlier, the Lagrange multipliers in (20) and (25) can quantify the effects of the changed constraints on the objectives F_1 and F_2. To avoid the different units of these multipliers, they should be normalized as λ_1' and λ_2' according to the discussions on λ_1 and λ_2. The basic values of I^2, S, CPQI for normalizing are $I_{h0}^2 + I_{q0}^2$, S_m, and σ, respectively. It should be note that λ_2 represents the sensitivity of CPQI F when capacity S changes as shown in (25), so the variable *dS/dF* of objective II should be the inverse of λ_2. Therefore, the *dS/dF* features of two objectives can be written as

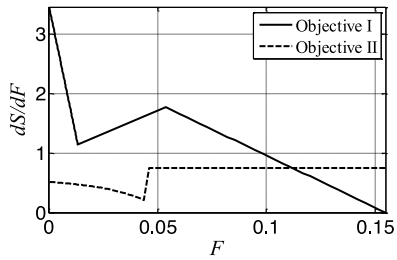

Fig. 15. Performances of two objectives on the sensitivity feature *dS/dF*.

$$(dS/dF)_1 = \lambda_1' = \lambda_1 \sigma / \left(I_{h0}^2 + I_{q0}^2\right) \tag{30}$$

$$(dS/dF)_2 = 1/\lambda_2' = \sigma/(\lambda_2 S_m) = \sigma \Big/ \left(\lambda_2 3U\sqrt{I_{h0}^2 + I_{q0}^2}\right) \tag{31}$$

where the subscripts "1" and "2" stand for objective I and II, respectively. According to (22), (27), (28), (30), and (31), the *dS/dF* features of the two objective-oriented control strategies can be obtained as depicted in Fig. 15. When the power quality is poor and CPQI is larger than 0.1118, the *dS/dF* feature of objective II is larger than the one of objective I. In such condition, objective I is recommended as the best usage because the increased compensation of the MFGTI is less sensitive to the changing of CPQI. On the contrary, when while the CPQI is less than 0.1118, objective II seems to be a better choice compared with objective I, since the *dS/dF* value of objective II is mostly less than one of objective I.

VI. Conclusion

To optimally handle the power quality issues in a microgrid using an MFGTI, an objective-oriented model is proposed in this paper based on AHP theory first. Then, the objectives to minimize the demanded capacity of the MFGTI (objective I) or minimize the CPQI (objective II) are presented. Furthermore, the solutions of such objectives are also given by means of Lagrange's theory. Finally, the experimental results performed on a feeder of a microgrid demonstration with two identical 10-kVA DGs have verified the validations and feasibility of the proposed models and control strategies. Some conclusions can be drawn as follows.

1) The grid-tied inverter in the microgrid has the auxiliary functionality to enhance the power quality of the microgrid, but the functionality is limited by the available margin capacity of the MFGTI. Thus, how to optimally organize and control the MFGTI is a very urgent necessary.
2) The proposed CPQI-based optimal model is simple and easy to carry out as an effective tool to quantify the power quality of the microgrid. It also can guide the optimal power quality compensation and the on-grid electricity price of microgrids in the power quality market in the near future.
3) Two objective-oriented optimal compensation strategies are proposed in this paper. One can confirm the minimum compensation capacity of MFGTI in the condition of the given CPQI; on the contrary, the other one can enhance the power quality of the microgrid as good as possible in the condition of given available capacity of the MFGTI. The comparative performances and the best usage of the two proposed control strategies are also discussed. These two objectives can flexibly adapt the applications of the MFGTIs in the microgrid and customize the power quality of the microgrid. It can be expected that this will be commonly applied to microgrids in the near future.

REFERENCES

[1] P. C. Loh, D. Li, Y. K. Chai, and F. Blaabjerg, "Autonomous operation of hybrid microgrid with AC and DC subgrids," *IEEE Trans. Power Electron.*, vol. 28, no. 5, pp. 2214–2223, May 2013.

[2] N. W. A. Lidula and A. D. Rajapakse, "Microgrids research: A review of experimental microgrids and test systems," *Renewable Sustainable Energy Rev.*, vol. 15, no. 1, pp. 186–202, Jan. 2011.

[3] Z. Zeng, R. Zhao, H. Yang, and S. Tang, "Policies and demonstrations of micro-grids in China: A review," *Renewable Sustainable Energy Rev.*, vol. 29, pp. 701–718, Jan. 2014.

[4] H. Nikkhajoei and R. H. Lasseter, "Distributed generation interface to the CERTS microgrid," *IEEE Trans. Power Del.*, vol. 24, no. 3, pp. 1598–1608, Jul. 2009.

[5] S. C. Tan, C. K. Lee, and S. Y. Hui, "General steady-state analysis and control principle of electric springs with active and reactive power compensations," *IEEE Trans. Power Electron.*, vol. 28, no. 8, pp. 3958–3969, Aug. 2013.

[6] J. He, Y. W. Li, F. Blaabjerg, and X. Wang, "Active harmonic filtering using current-controlled, grid-connected DG units with closed-loop power control," *IEEE Trans. Power Electron.*, vol. 29, no. 2, pp. 642–653, Feb. 2014.

[7] J. H. R. Enslin and P. J. M. Heskes, "Harmonic interaction between a large number of distributed power inverters and the distribution network," *IEEE Trans. Power Electron.*, vol. 19, no. 6, pp. 1586–1593, Nov. 2004.

[8] J. He, Y. W. Li, D. Bosnjak, and B. Harris, "Investigation and active damping of multiple resonances in a parallel-inverter-based microgrid," *IEEE Trans. Power Electron.*, vol. 28, no. 1, pp. 234–246, Jan. 2013.

[9] H. Xu, J. Hu, and Y. He, "Operation of wind-turbine-driven DFIG systems under distorted grid voltage conditions: Analysis and experimental validations," *IEEE Trans. Power Electron.*, vol. 27, no. 5, pp. 2354–2366, May 2012.

[10] J. Driesen, T. Green, T. Van Craenenbroeck, and R. Belmans, "The development of power quality markets," in *Proc. IEEE PES Winter Meet.*, 2002, pp. 262–267.

[11] Z. Zeng, R. Zhao, H. Yang, and C. Cheng, "Topologies and control strategies of multi-functional grid-connected inverters for power quality enhancement: A comprehensive review," *Renewable Sustainable Energy Rev.*, vol. 24, pp. 223–270, Aug. 2013.

[12] Z. Zou, Z. Wang, and M. Cheng, "Modeling, analysis, and design of multifunction grid-interfaced inverters with output LCL filter," *IEEE Trans. Power Electron.*, vol. 29, no. 7, pp. 3830–3839, Jul. 2013.

[13] J. C. Vasquez, R. A. Mastromauro, J. M. Guerrero, and M. Liserre, "Voltage support provided by a droop-controlled multifunctional inverter," *IEEE Trans. Ind. Electron.*, vol. 56, no. 11, pp. 4510–4519, Nov. 2009.

[14] R. I. Bojoi, L. R. Limongi, D. Roiu, and A. Tenconi, "Enhanced power quality control strategy for single-phase inverters in distributed generation systems," *IEEE Trans. Power Electron.*, vol. 26, no. 3, pp. 798–806, Mar. 2011.

[15] J. Miret, A. Camacho, M. Castilla, L. G. de Vicuna, and J. Matas, "Control scheme with voltage support capability for distributed generation inverters under voltage sags," *IEEE Trans. Power Electron.*, vol. 28, no. 11, pp. 5252–5262, Nov. 2013.

[16] S. Dasgupta, S. K. Sahoo, and S. K. Panda, "Single-phase inverter control techniques for interfacing renewable energy sources with microgrid—Part I: Parallel-connected inverter topology with active and reactive power flow control along with grid current shaping," *IEEE Trans. Power Electron.*, vol. 26, no. 3, pp. 717–731, Mar. 2011.

[17] F. Wang, J. L. Duarte, and M. A. M. Hendrix, "Pliant active and reactive power control for grid-interactive converters under unbalanced voltage dips," *IEEE Trans. Power Electron.*, vol. 26, no. 5, pp. 1511–1521, May 2011.

[18] Y. W. Li, D. M. Vilathgamuwa, and P. C. Loh, "A grid-interfacing power quality compensator for three-phase three-wire microgrid applications," *IEEE Trans. Power Electron.*, vol. 21, no. 4, pp. 1021–1031, Jul. 2006.

[19] B. Han, B. Bae, H. Kim, and S. Baek, "Combined operation of unified power-quality conditioner with distributed generation," *IEEE Trans. Power Del.*, vol. 21, no. 1, pp. 330–338, Jan. 2006.

[20] Z. Zeng, R. X. Zhao, and H. Yang, "Coordinated control of multifunctional grid-tied inverters using conductance and susceptance limitation," *IET Power Electron.*, 2014.

[21] R. R. Sawant and M. C. Chandorkar, "A multifunctional four-leg grid-connected compensator," *IEEE Trans. Ind. Appl.*, vol. 45, no. 1, pp. 249–259, Jan./Feb. 2009.

[22] T. Wu, H. Nien, H. Hsieh, and C. Shen, "PV power injection and active power filtering with amplitude-clamping and amplitude-scaling algorithms," *IEEE Trans. Ind. Appl.*, vol. 43, no. 3, pp. 731–741, May/Jun. 2007.

[23] K. J. P. Macken, K. Vanthournout, J. Van den Keybus, G. Deconinck, and R. J. M. Belmans, "Distributed control of renewable generation units with integrated active filter," *IEEE Trans. Power Electron.*, vol. 19, no. 5, pp. 1353–1360, Sep. 2004.

[24] C. Cheng, Z. Zeng, H. Yang, and R. X. Zhao, "Multi-objective optimal compensation of a multi-functional grid-connected inverter for power quality enhancement," in *Proc. IEEE Int. Conf. Electr. Mach. Syst.*, 2012, pp. 1–6.

[25] E. Twining and D. G. Holmes, "Grid current regulation of a three-phase voltage source inverter with an LCL input filter," *IEEE Trans. Power Electron.*, vol. 18, no. 3, pp. 888–895, May 2003.

[26] Y. Jia, J. Zhao, and X. Fu, "Direct grid current control of LCL-filtered grid-connected inverter mitigating grid voltage disturbance," *IEEE Trans. Power Electron.*, vol. 29, no. 3, pp. 1532–1541, Mar. 2014.

[27] C. Bao, X. Ruan, X. Wang, W. Li, D. Pan, and K. Weng, "Step-by-step controller design for LCL-type grid-connected inverter with capacitor-current-feedback active-damping," *IEEE Trans. Power Electron.*, vol. 29, no. 3, pp. 1239–1253, Mar. 2014.

[28] N. Bhushan and K. Rai, *Strategic Decision Making: Applying the Analytic Hierarchy Process*. London, U.K.: Springer-Verlag, 2004.

[29] J. M. Guerrero, J. C. Vasquez, J. Matas, L. G. de Vicuna, and M. Castilla, "Hierarchical control of droop-controlled AC and DC microgrids—A general approach toward standardization," *IEEE Trans. Ind. Electron.*, vol. 58, no. 1, pp. 158–172, Jan. 2011.

[30] J. M. Guerrero, M. Chandorkar, T. Lee, and P. C. Loh, "Advanced control architectures for intelligent microgrids—Part I: Decentralized and hierarchical control," *IEEE Trans. Ind. Electron.*, vol. 60, no. 4, pp. 1254–1262, Apr. 2013.

Zheng Zeng (S'14) received the B.Sc. degree from Wuhan University, China, in 2009. He is currently working toward the Ph.D. degree at Zhejiang University, Hangzhou, China.

His current research interests include microgrid and distributed generation, grid-connected inverter, and power quality.

Huan Yang (M'09) received the B.Sc. and Ph.D. degrees in electrical engineering and its automation and electrical engineering from Zhejiang University, Hangzhou, China, in 2003 and 2008, respectively.

From January 2009 to March 2011, he was a Postdoctoral Fellow at the College of Electrical Engineering, Zhejiang University. In March 2011, he became a faculty member in Zhejiang University as a Research Associate and promoted to an Associate Professor in December 2012. From April 2012 to April 2013, he conducted joint research in Fuji Electric Co., Ltd., as the Oversea Researcher of New Energy and Industrial Technology Development Organization, Tokyo, Japan. His research interests include motor drives and grid-connected converter in microgrids.

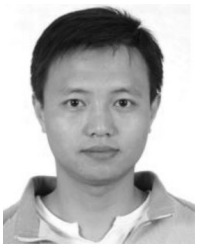

Shengqing Tang received the B.Sc. degree from Hunan University, Changsha, China, in 2003, and the M.Sc. degree from South China University of Technology, Guangzhou, China, in 2006. He is currently working toward the Ph.D. degree at Zhejiang University, Hangzhou, China.

His current research interests include microgrid, power quality, energy storage, and grid-tied inverter.

Rongxiang Zhao received the B.Sc., M.Sc., and Ph.D. degrees in electrical engineering from Zhejiang University, Hangzhou, China, in 1984, 1987, and 1991, respectively.

He is a Full Professor of the College of Electrical Engineering, Zhejiang University, where he is also the Director of the National Engineering Research Center for Applied Power Electronics, Industrial Technology Research Institute of Zhejiang University, and Zhejiang University and Fuji Electric Innovation Center. His current research interests include motor control, power converter systems, renewable energy and distributed generation, and energy storage.